BIOCHEMISTRY
including biophysical chemistry & molecular biology

Article

pubs.acs.org/biochemistry

Uncovering the Mechanism of Forkhead-Associated Domain-Mediated TIFA Oligomerization That Plays a Central Role in Immune Responses

Jui-Hung Weng,[†,‡,§] Yin-Cheng Hsieh,[∥] Chia-Chi Flora Huang,[†,‡,⊥] Tong-You Wade Wei,[†,⊥] Liang-Hin Lim,[†,⊥] Yu-Hou Chen,[†] Meng-Ru Ho,[†] Iren Wang,[†] Kai-Fa Huang,[†] Chun-Jung Chen,[∥] and Ming-Daw Tsai*[,†,‡,⊥]

[†]Institute of Biological Chemistry, Academia Sinica, Taipei, Taiwan
[‡]Taiwan International Graduate Program, Academia Sinica, Taipei, Taiwan
[§]Institute of Biochemical Sciences, Department of Chemistry, National Tsing Hua University, Hsinchu, Taiwan
[∥]Life Science Group, Scientific Research Division, National Synchrotron Radiation Research Center, Hsinchu, Taiwan
[⊥]Institute of Biochemical Sciences, National Taiwan University, Taipei, Taiwan

ABSTRACT: Forkhead-associated (FHA) domain is the only signaling domain that recognizes phosphothreonine (pThr) specifically. TRAF-interacting protein with an FHA domain (TIFA) was shown to be involved in immune responses by binding with TRAF2 and TRAF6. We recently reported that TIFA is a dimer in solution and that, upon stimulation by TNF-α, TIFA is phosphorylated at Thr9, which triggers TIFA oligomerization via pThr9−FHA domain binding and activates nuclear factor κB (NF-κB). However, the structural mechanism for the functionally important TIFA oligomerization remains to be established. While FHA domain−pThr binding is known to mediate protein dimerization, its role in oligomerization has not been demonstrated at the structural level. Here we report the crystal structures of TIFA (residues 1−150, with the unstructured C-terminal tail truncated) and its complex with the N-terminal pThr9 peptide (residues 1−15), which show unique features in the FHA structure (intrinsic dimer and extra β-strand) and in its interaction with the pThr peptide (with residues preceding rather than following pThr). These structural features support previous and additional functional analyses. Furthermore, the structure of the complex suggests that the pThr9−FHA domain interaction can occur only between different sets of dimers rather than between the two protomers within a dimer, providing the structural mechanism for TIFA oligomerization. Our results uncover the mechanism of FHA domain-mediated oligomerization in a key step of immune responses and expand the paradigm of FHA domain structure and function.

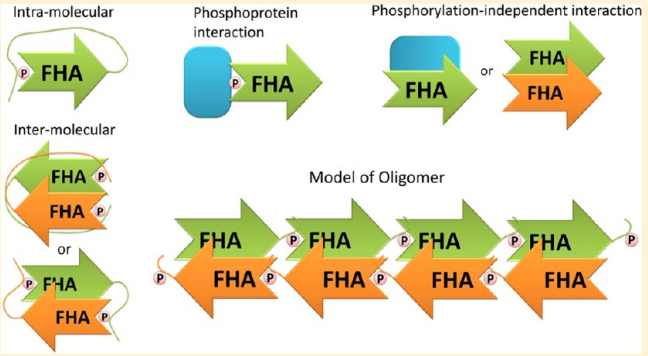

Forkhead-associated (FHA) domain was first discovered in 1995[1] and later recognized for its unique structural feature[2,3] and specificity for binding phosphothreonine (pThr).[3−5] This protein−phosphoprotein interaction motif is conserved in prokaryotes and eukaryotes.[6] However, the flanking residues are much more diverse,[7,8] and phosphorylation-independent interactions have also been reported.[9,10] In contrast to its highly conserved β-sandwich architecture, which is composed of a five-stranded β-sheet and a six-stranded β-sheet, the loops connecting β-strands vary in length. Furthermore, FHA domains overall have a relatively low level of sequence homology. Only a few conserved residues could be recognized at the pThr binding region, and no pattern could be identified within the β-strands.[6,11] Many studies have suggested that FHA domains play major roles in a range of biological functions such as cell cycle controls, and DNA damage repair and transductions. In addition, different functions and mechanisms of pThr−FHA domain interactions have been reported, including the most common protein−phosphoprotein interaction between two different proteins[3,12] (Figure 1A), intramolecular pThr−FHA domain interaction resulting in autoinhibition[13] (Figure 1B), intermolecular pThr−FHA domain interaction between two molecules of the same protein, which could facilitate dimerization of FHA domain-containing proteins in head-to-tail[14−16] or head-to-head[17,18] configurations (Figure 1C), and phosphorylation-independent interactions that could also mediate protein−protein interaction[9] or dimerization[10] (Figure 1D).

Received: May 6, 2015
Revised: September 16, 2015
Published: September 21, 2015

DOI: 10.1021/acs.biochem.5b00500
Biochemistry 2015, 54, 6219−6229

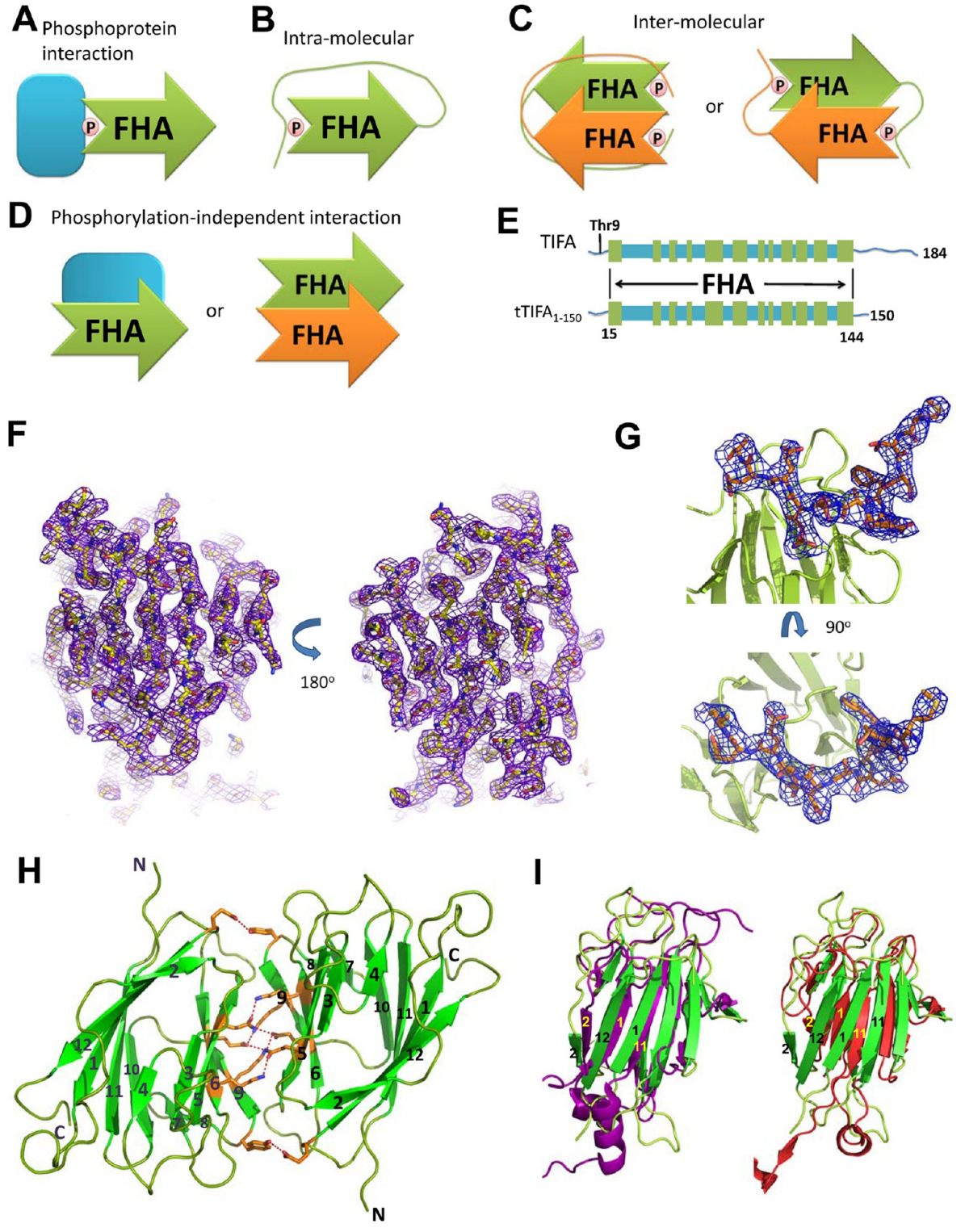

Figure 1. Overall structural features of the TIFA FHA domain. (A–D) Different mechanistic models of FHA domain interactions: FHA domain binding to another protein containing pThr (A), intramolecular binding of FHA domain with its own N-terminal pThr (B), intermolecular binding of FHA domain with another monomer to facilitate dimerization (C), and phosphorylation-independent functions mediating protein–protein interaction or dimerization (D). (E) Schematic overview of TIFA and truncated TIFA. Green-colored boxes indicate β-strands. N- and C-terminal unstructured regions are colored blue. (F) The $2F_o - F_c$ electron density map around the FHA domain of the $tTIFA_{1-150}$ structure overlaid with the final refined model. The map is contoured at the 0.9σ level. All built residues fitted well to the density. (G) The $2F_o - F_c$ electron density map around the bound phosphopeptide in the $tTIFA_{1-150}$-pThr9-$TIFA_{1-15}$ structure overlaid with the final refined model. The map is contoured at the 0.9σ level. All built residues in the peptide fitted well to the density. (H) Dimer structure of $tTIFA_{1-150}$ with β-strands labeled. Residues involved in dimerization are shown as sticks. (I) Structure alignment between TIFA (green) and Rad53 FHA1 (PDB entry 1G6G)[3] (left, purple) or NBS1 FHA (PDB entry 3HUF)[43] (right, red).

DOI: 10.1021/acs.biochem.5b00500
Biochemistry 2015, 54, 6219–6229

TIFA is involved in the activation of nuclear factor κB (NF-κB) by various stimulations such as tumor necrosis factor α (TNF-α), interleukin-1 (IL-1), lipopolysaccharide (LPS), and hypoxia.[19−21] It has been demonstrated that in the absence of upstream signals, TIFA overexpression is sufficient to activate NF-κB and c-Jun amino-terminal kinase (JNK). These studies suggested that the activation is the result of enhanced interaction of TRAF6 with IL-1 receptor-associated kinase 1 (IRAK-1). Furthermore, *in vitro* studies indicate that IκB kinase (IKK) can be activated by the oligomeric form of TIFA through the promotion of TRAF6 oligomerization and ubiquitination.[22] A paper just published in *Science* also reported that TIFA is crucial for initiating innate immune responses triggered by bacterially derived monosaccharide heptose 1,7-bisphosphate.[23]

We previously showed that recombinant TIFA is dimeric in solution, and that Thr9 of TIFA is phosphorylated upon stimulation by TNF-α.[24] We proposed that this phosphorylation triggers TIFA oligomerization via pThr9−FHA domain binding between dimers of TIFA, leading to TNF-α-mediated NF-κB activation.[24] To gain structural and mechanistic insight into TIFA self-association, we report the long-awaited structure of TIFA ($tTIFA_{1-150}$) and its complex with TIFA N-terminally phosphorylated Thr9 peptide 1−15 (pThr9-$TIFA_{1-15}$). The results show novel structural features of TIFA and reveal the molecular mechanism for the functionally important oligomerization of TIFA.

MATERIALS AND METHODS

Protein Expression and Purification. Different tags, including GST, MBP, and His, were fused with various C-terminally truncated TIFAs such as residues 1−135, 1−150, or 1−163 for screening. The truncated recombinant TIFA protein constructs shorter than 150 residues failed to be overexpressed in the soluble form. We used the 1−150 construct with His tag for the structural study because of its high expression levels. Expressions of the recombinant TIFA protein and selenomethionine-substituted His-$tTIFA_{1-150}$ (SeMet $tTIFA_{1-150}$) were conducted using *Escherichia coli* expression strain BL21 codon plus. The expression culture was grown at 37 °C to an OD_{600} of 0.8. The temperature was then reduced to 16 °C, and expression was induced by the addition of isopropyl β-D-1-thiogalactopyranoside (IPTG) to a final concentration of 0.5 mM. The cells were harvested 16 h after induction, and pellets were resuspended in binding buffer [200 mM NaCl, 10 mM imidazole, and 50 mM Tris-HCl (pH 8.0)]. The proteins were initially purified using a self-packed Ni^{2+} resin (Millipore) column. The Ni^{2+} resin was equilibrated in binding buffer before the sample was loaded into the column. The column was washed with washing buffer [200 mM NaCl, 80 mM imidazole, and 50 mM Tris-HCl (pH 8.0)] and then eluted with elution buffer [200 mM NaCl, 400 mM imidazole, and 50 mM Tris-HCl (pH 8.0)]. The eluent was concentrated and further purified with a HiLoad 16/60 Superdex 75 column (GE Healthcare) pre-equilibrated with binding buffer. The separated fractions were analyzed by 15% sodium dodecyl sulfate−polyacrylamide gel electrophoresis (SDS−PAGE), and proteins were visualized by Coomassie blue staining. The purified protein was collected and concentrated to 16 mg mL^{-1} for crystallization trials. SeMet $tTIFA_{1-150}$ was prepared by changing the culture medium to M9 medium containing 10 mg L^{-1} selenomethionine before IPTG induction. After purification as described above, the protein was exchanged into final crystallization buffer [150 mM NaCl and 50 mM citric acid (pH 5.5)].

The mutants used in dimer breaking and phosphopeptide binding experiments were all full-length TIFA and were purified as described above.

Crystallization and Data Collection. Initial crystallization screens were conducted by the sitting drop vapor-diffusion method using a Phoenix crystallization robot. A protein solution (0.5 μL) was mixed with 0.5 μL of a crystallization solution and equilibrated with a 70 μL reservoir at 277 K. Optimization of the crystals was performed with different combinations of Hampton additive screening kits. The crystallization buffer for SeMet $tTIFA_{1-150}$ consisted of 80 mM LiCl, 0.2 M trimethylamine *N*-oxide, 15% PEG 3350, and 100 mM HEPES (pH 7.0). Extra PEG 3350 was added to a final concentration of 30% as a cryoprotectant. Crystals of the SeMet $tTIFA_{1-150}$ complex with pThr9-$TIFA_{1-15}$ were obtained by cocrystallization of a 2-fold excess of the peptide with the SeMet $tTIFA_{1-150}$ protein in 2.1 M DL-malic acid (pH 7.0). The crystals of SeMet $tTIFA_{1-150}$-pThr9-$TIFA_{1-15}$ did not require additional cryoprotectant. X-ray diffraction data were collected at beamline 13B1 of the National Synchrotron Radiation Research Center (Hsinchu, Taiwan) and beamline 44XU of SPring-8 (Hyogo, Japan). Se-SAD/MAD data sets were collected at 110 K using wavelengths of 0.9791 Å (edge) and 0.9640 Å (high remote). Diffraction intensities were integrated and scaled with the HKL2000 package.[25]

Structural Determination and Refinement. The procedures are highlighted briefly in Results, and additional details are provided here. At first, all crystals were thin and sensitive to radiation damage. Therefore, only single-wavelength (edge) data were available for SAD phase determination. The selenium sites of SeMet $tTIFA_{1-150}$ were located with SHELX C/D/E,[26] and the initial phase was calculated by Phaser[27] followed by density modification with DM.[28] Then the optimal initial phases were determined by the direct phase selection method to reduce the phase ambiguity,[29] and subsequently, automated model building was performed with Buccaneer.[30] The model was further improved by conventional two-wavelength MAD data sets collected from optimized crystals. The final model was built and refined manually with COOT and Refmac5.[31−33] Using the structure of SeMet $tTIFA_{1-150}$ as the starting model, the structure of the complex form, SeMet $tTIFA_{1-150}$-pThr9-$TIFA_{1-15}$, was then determined by molecular replacement with Phaser-MR of the PHENIX package.[34] Model building and refinement procedures were the same as those described above. Structural presentations were generated using PyMol.[35] All residues, except for the first eight residues and the C-terminal tag, were readily visible in the electron density map.

Cell Culture and Co-immunoprecipitation Analysis. 293T cells were maintained in a humidified atmosphere at 37 °C with 5% CO_2 in high-glucose Dulbecco's modified Eagle's medium (DMEM, Gibco) supplemented with 10% fetal bovine serum (Gibco), 2 mM L-glutamine, 125 units mL^{-1} streptomycin, and 125 μg mL^{-1} penicillin. A half million cells were cotransfected with 3 μg each of the vectors expressing Flag-tagged TIFA (WT) and Myc-tagged TIFA (WT or mutants) using Jet-PEI (Polyplus Transfection). After 36 h, cells were lysed with TNE buffer [10 mM Tris-HCl (pH 7.8), 1% NP-40, 0.15 M NaCl, and 1 mM EDTA] supplemented with protease inhibitor cocktail (Roche) and phosphatase inhibitor cocktails (Sigma-Aldrich). The cell lysates were incubated with Dynabeads precoated by a Flag- or Myc-specific

DOI: 10.1021/acs.biochem.5b00500
Biochemistry 2015, 54, 6219−6229

Table 1. Data Collection and Refinement Statistics[a]

	$tTIFA_{1-150}$ (PDB entry 4ZGI)		$tTIFA_{1-150}$-pThr9-$TIFA_{1-15}$ (PDB entry 4YM4)
	Data Collection		
space group	$P3_221$		$P4_232$
cell dimensions [*a*, *b*, *c* (Å)]	39.0, 39.0, 178.5		113.1, 113.1, 113.1
	edge	high remote	
wavelength (Å)	0.9791	0.9640	1.0
resolution (Å)	20−2.70 (2.80−2.70)	20−2.70 (2.80−2.70)	20−3.12 (3.23−3.12)
no. of unique reflections	4730	4744	2375
R_{sym} or R_{merge}	0.068 (0.596)	0.071 (0.678)	0.034 (0.186)
$\langle I/\sigma(I)\rangle$	18.7 (6.8)	19.5 (7.5)	25.6 (4.7)
completeness (%)	98.1 (95.0)	98.3 (97.9)	100.0 (100.0)
redundancy	8.8 (6.4)	8.9 (7.0)	20.7 (19.8)
	Refinement		
resolution (Å)	20−2.70		20−3.12
no. of reflections/test set	4730/409		4775/226
R_{work}, R_{free} (%)	24.6, 28.1		21.3, 23.9
no. atoms/*B* factor (Å^2)			
protein	1156/40.7		1144/41.3
peptide	–		96/78.1
water	8/33.1		–
mean *B* value (Å^2)	40.6		44.6
Wilson *B* value (Å^2)	35.2		65.0
root-mean-square deviation			
bond lengths (Å)	0.012		0.027
bond angles (deg)	1.17		1.97
Ramachandran plot (%)			
preferred regions	95.65		95.97
allowed regions	4.35		4.03
outliers	0		0

[a]Values in parentheses are for the highest-resolution shell.

antibody (Sigma-Aldrich) at 4 °C overnight and then washed with PBS-T buffer (PBS supplemented with 0.1% Tween 20). Precipitated proteins were then eluted with Laemmli sample buffer [50 mM Tris-HCl (pH 6.8), 10% glycerol, 1% SDS, 300 mM 2-mercaptoethanol, and 0.01% bromophenol blue], separated by SDS−PAGE (12% polyacrylamide), and blotted onto Immobilon-P polyvinylidene difluoride membranes (Millipore). Membranes were then blocked for 1 h with 5% dry milk in PBS-T buffer and incubated overnight at 4 °C with a primary antibody diluted in PBS containing 1% BSA (Sigma-Aldrich). After three washes with PBS-T, membranes were incubated for 1 h with secondary antibodies in PBS-T and then washed five times with PBS-T. The immunoblots were visualized by enhanced chemiluminescence (Westernbright ECL, Advansta).

Size Exclusion Chromatography−Multiangle Light Scattering (SEC−MALS). The molecular weight of TIFA WT was determined by static light scattering (SLS) using a Wyatt Dawn Heleos II multiangle light scattering detector (Wyatt Technology) coupled with an AKTA Purifier UPC10 FPLC protein purification system; 2.0 mg mL^{-1} TIFA protein (100 μL) was subjected to a Superdex 75 5/150 GL size exclusion column (GE) with a buffer [200 mM NaCl, 50 mM Tris-HCl, and 0.02% NaN_3 (pH 8.0)], at a rate of 0.5 mL min^{-1}. The refractive index was measured with a Wyatt Optilab T-rEX instrument connected downstream of the LS detector.

Analytical Ultracentrifugation (AUC). AUC analysis was performed using an An-60 or An-50 Ti rotor on a Beckman Coulter (Fullerton, CA) XL-I instrument. Proteins (20 μM) and buffers were loaded into a 12 mm standard double-sector Epon charcoal-filled centerpiece. The experiment was performed at 20 °C and a rotor speed of 40000 rpm, and the signal was monitored at 280 nm. The raw experimental data were analyzed by Sedfit (http://www.analyticalultracentrifugation.com/default.htm), and the plots of *c*(*s*,fr) and molecular mass versus the *s* value were generated by MATLAB (MathWorks, Inc.).

Isothermal Titration Calorimetry (ITC) Analysis. ITC experiments were performed as described previously.[24] After thermal equilibration at 25 °C, a single 1 μL injection and 19 serial injections of 2 μL of peptide (3 mM) were titrated into a calorimeter cell (0.2044 mL) containing TIFA protein (0.2 mM). Three $TIFA_{1-15}$ peptides, pT9-$TIFA_{1-15}$ [MTSFEDAD-(pT)EETVTC], E5A pT9-$TIFA_{1-15}$ [MTSFADAD(pT)EET-VTC], and $TIFA_{1-15}$ (MTSFEDADTEETVTC), were used to titrate TIFA proteins (WT or S53A mutant). Identical injections of the peptide into the protein buffer were performed to measure the heats of dilution from titrants, and these values were subtracted from each titration. Each titration was repeated three times, and thermal data were fitted to a standard one-protomer, one-binding site model to yield the K_d value.

Biolayer Interferometry by the Octet Systems. Binding affinities of TIFA, WT and mutants, for pThr peptide were measured by biolayer interferometry (ForteBio) at 30 °C. Recombinant His-TIFA was immobilized on the NTA biosensor tips in the starting buffer [200 mM NaCl and 50 mM Tris-HCl (pH 8.0)]. To avoid nonspecific interactions, 0.5% Tween 20 was added to assay buffer [200 mM NaCl, 50 mM Tris-HCl, and 0.5% Tween 20 (pH 8.0)]. The association and dissociation binding kinetics for pThr peptides were

DOI: 10.1021/acs.biochem.5b00500
Biochemistry 2015, 54, 6219−6229

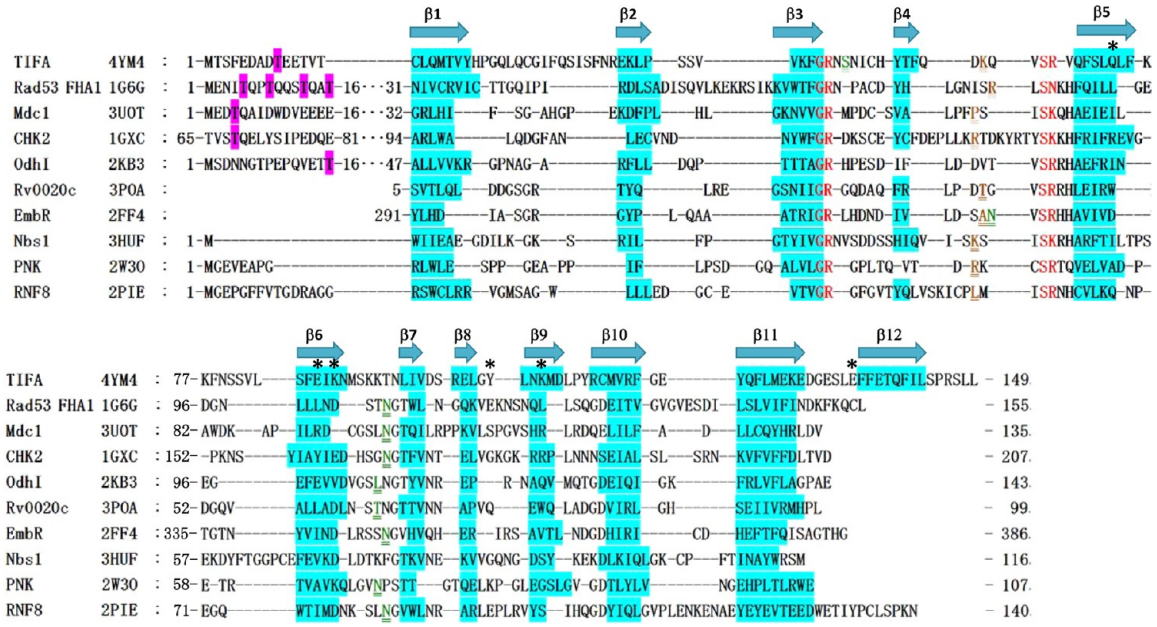

Figure 2. Structure-based sequence alignment of the TIFA FHA domain and other FHA domains. The FHA domains for comparison include Rad53 FHA1,[3] Mdc1,[15] CHK2,[14] OdhI,[13] Rv0020c,[3] EmbR,[44] Nbs1,[43] PNK,[45] and RNF8.[46] The β-strands are highlighted in blue. Self-recognition pThr sites are highlighted in purple. The conserved GR and S(R/K/N) pThr binding motifs are colored red. Residues that form a hydrogen bond between their carbonyl group and the amino group from the +1 residue on the peptide are colored brown. Residues involved in additional recognitions are colored green. Residues at the dimer interface are highlighted with stars.

measured by placing TIFA-coated biosensor tips into five wells that contained 3-fold serially diluted peptide (frmo 3 to 0.037 mM). All data were processed using Fortebio software for the steady state K_d values.

RESULTS AND DISCUSSION

Structural Determination by Using the New Direct Phase Selection Method. Because we (and others) have encountered unusual difficulty in determining the structure of TIFA, the procedures are highlighted here briefly (with additional details in Materials and Methods). The full-length TIFA consists of 184 amino acids, including an FHA domain flanked by a disordered region at both N- and C-termini based on HHpred prediction[36] (Figure 1E). We screened expression and crystallization conditions for the full-length and several different C-terminally truncated forms of TIFA with various tags and found that the construct with residues 1−150 (tTIFA$_{1-150}$) could be overexpressed in *E. coli* with a His tag at the C- or N-terminus. However, only the one with a C-terminal His tag could be crystallized. The SeMet-labeled recombinant protein and its complex with pThr9-TIFA$_{1-15}$ (residues 1−15) were also successfully crystallized. However, determination of the structures was unsuccessful when the conventional SAD programs were used to calculate and refine the phases. Model refinement based on known FHA domains was also unfeasible because of the variation in loop regions among FHA domains. Finally, the recently developed direct phase selection method[29] effectively resolved the ambiguity of SAD phases and generated optimized initial phases for structure determination. The new algorithm is particularly helpful in cases where only SAD data are available. Subsequently, the structure of the complex was determined by molecular replacement (MR). The structural statistics of both structures are listed in Table 1.

As described in the following sections, both structures display several unique structural features, including being dimers. Figure 1F shows the $2F_o - F_c$ map of the tTIFA$_{1-150}$ structure, indicating that all residues were built on the basis of the clear electron density, whereas Figure 1G shows the clear and continuous $2F_o - F_c$ map of the peptide (residues 1−12) of the tTIFA$_{1-150}$-pThr9-TIFA$_{1-15}$ structure.

Unusual Structural Architecture of the TIFA FHA Domain. To date, 77 FHA domain structures from 38 different proteins have been reported on the basis of the PDB. Similar to typical FHA domains, tTIFA$_{1-150}$ adopts a β-sandwich scaffold composed of two β-sheets. However, the FHA domain of TIFA has one additional strand, β12, that makes it unique (Figure 1H). Figure 1I shows the comparison of TIFA with two other FHA domains. In typical FHA domains, one β-sheet of the β-sandwich is composed of antiparallel β2, β1, β11, β10, β7, and β8 strands, and the other contains five mixed β-strands (β4, β3, β5, β6, and β9). However, both β-sheets of the TIFA FHA domain are mixed. Strand β12 of TIFA inserts between strands β1 and β2 (parallel to β1 and antiparallel to β2) and is fully incorporated into the architecture of the β-sandwich. This also results in a broader β-sheet. In addition, the TIFA FHA domain has an unusually long loop connecting strands β1 and β2.

Figure 2 shows the structure-based sequence alignment of TIFA FHA with some of the well-characterized FHA domains. It is clear from this alignment that β12 is a unique feature of TIFA. Though β12 is not conserved, its importance in the structural integrity of TIFA is supported by our finding that a shorter construct of TIFA (residues 1−135) designed according to the canonical FHA structure could not be expressed with a variety of tags in a stable form. This could also explain why the structure of TIFA FHA has not been reported until now, despite the fact that several significant functional studies have already been published.[19−24,37,38]

DOI: 10.1021/acs.biochem.5b00500
Biochemistry 2015, 54, 6219−6229

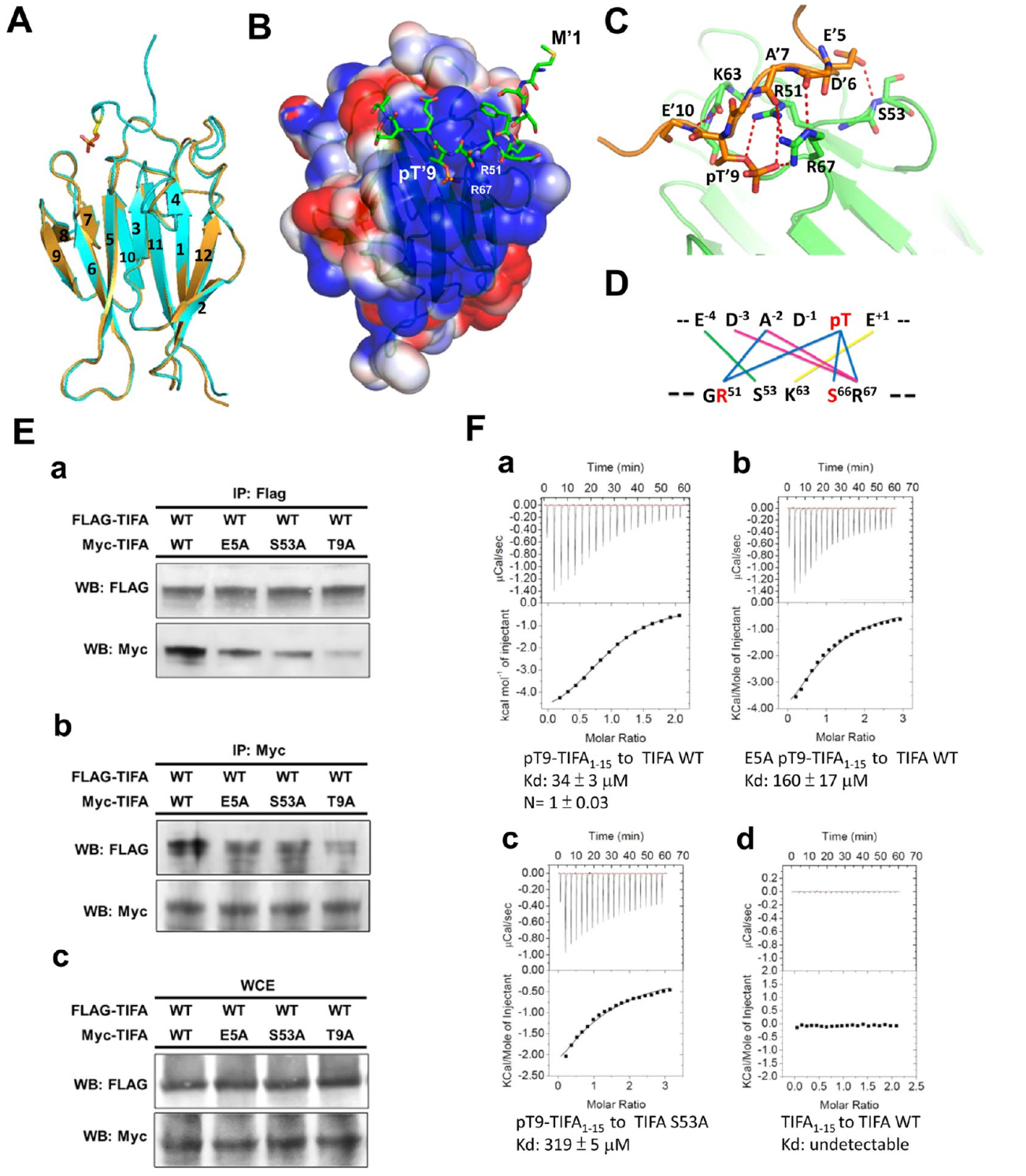

Figure 3. Structure of the TIFA complex with its N-terminally phosphorylated Thr9 peptide 1−15. (A) Superposition of $tTIFA_{1-150}$ (orange) and $tTIFA_{1-150}$-pThr9-$TIFA_{1-15}$ (cyan). pThr9 is shown as sticks. (B) Electrostatic surface potential of $tTIFA_{1-150}$ (scale from −1 to +1 kT/e; blue, positive; red, negative). The bound peptide is shown as sticks. (C) Interaction between the pThr peptide and the TIFA FHA domain. (D) Schematic presentation of the interactions in panel C. (E) Flag-tagged TIFA WT and Myc-tagged TIFA (WT, E5A, S53A, or T9A) were cotransfected in HEK 293T cells and subjected to immunoprecipitation using both Flag-specific (a) and Myc-specific (b) immuno-beads, respectively. The precipitated proteins were eluted by sample buffer and analyzed through Western blotting using Myc-specific and Flag-specific antibodies, respectively. The whole cell extracts (WCE) used as IP inputs are also shown (c). (F) Use of ITC to test the effect of Ser53−Glu5 interaction on ligand binding affinity. The dissociation constant (K_d) between pT9-$TIFA_{1-15}$ and TIFA WT is 33.6 ± 2.9 μM with N = 1 ± 0.03 (one peptide to one protomer) (a). Because of the limitation in the working concentration of the peptide as a result of weaker binding, N = 1 was assumed in the experiments of the other two samples, which gave a K_d of 160 ± 17 μM for E5A pT9-$TIFA_{1-15}$ binding to TIFA WT (b) and is 319 ± 5 μM for pT9-$TIFA_{1-15}$ binding to TIFA S53A (c). Omission of phosphorylation abolished binding (d).

DOI: 10.1021/acs.biochem.5b00500
Biochemistry 2015, 54, 6219−6229

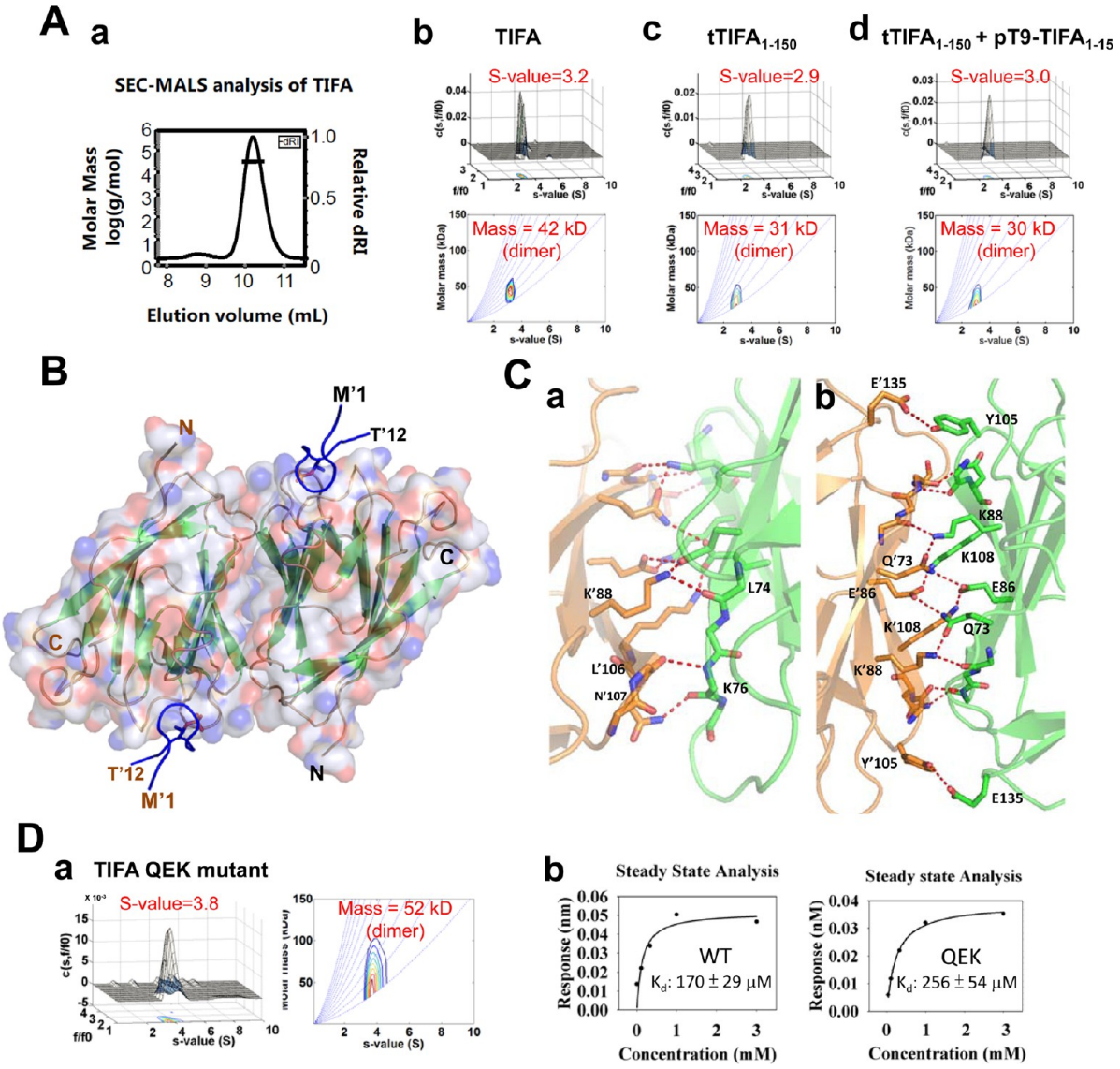

Figure 4. Dimer interface of TIFA. (A) Additional evidence of the dimerization state of TIFA in solution: (a) SEC−MALS analysis showing full-length TIFA as a monodispersed dimer in solution with a molecular weight of 44.15 kDa, (b) AUC of full-length TIFA, (c) AUC of $tTIFA_{1-150}$, and (d) AUC of the $tTIFA_{1-150}$-pThr9-$TIFA_{1-15}$ complex. (B) Crystal structure of the SeMet $tTIFA_{1-150}$ dimer in complex with pThr9-$TIFA_{1-15}$. The pThr9 peptides are shown as sticks. (C) Interactions at the dimer interface. (a) Hydrogen bonding involving the backbone. (b) Hydrogen bonding and ionic bonds between side chains. (D) AUC results of Q73A/E86A/K108A (QEK mutant) showing that it remained a dimer (a). In addition, the K_d measured by Octet showed that the binding affinity of QEK for pThr9-$TIFA_{1-15}$ is similar to that of WT (b). The binding is weaker compared to the ITC result (based on the WT data) possibly because of different conditions (e.g., 0.5% Tween 20 was added in the assay buffer of Octet experiments).

The Structure of the TIFA Complex with pThr9-$TIFA_{1-15}$ Indicates a Novel Mode of Ligand Binding. In agreement with other FHA domains, the binding of pThr peptide does not substantially alter the structure. As shown in Figure 3A, the structures of $tTIFA_{1-150}$ and $tTIFA_{1-150}$-pThr9-$TIFA_{1-15}$ are very similar, and superposition of the two structures results in a root-mean-square deviation (rmsd) of 0.47 Å (128 atoms). The small deviation comes from the $\beta1-\beta2$ loop and a slight bend at the end of $\beta12$. As also shown in Figure 2, the residues important for pThr binding are also conserved in TIFA. Like other FHA domains, conserved residues Arg51, Ser66, and Arg67 form H-bonds with pThr9. As shown in Figure 3B, residues Phe4′−Glu10′ of the bound pThr peptide are in contact with the positive electrostatic surface involving Arg51 and Arg67. Specific interactions between TIFA FHA and the bound pThr peptide are shown in Figure 3C.

For the FHA domains that recognize pThr, our review in 2008[6] suggested four types of FHA domain−ligand interactions (in addition to pThr): (i) the "pT+3" type where the interaction is mainly at the +3 residue after pThr, (ii) The "N- and C-termini to pT" type where the interaction occurs at both sides of pThr, (iii) the "pT-pT+3" like Dun1 FHA that interacts with two pThr residues and the +3 position of the second pThr,[39] and (iv) The "pT + an extended binding surface" type like Ki67 FHA.[40] Examination of Figure 3C indicates that TIFA FHA−ligand interaction represents a distinct type, where the interactions occur mainly with residues N-terminal to pThr (−4 to +1) as illustrated in Figure 3D. As explained below, the residues from pT+3 are an integral part of

DOI: 10.1021/acs.biochem.5b00500
Biochemistry 2015, 54, 6219−6229

the FHA domain and thus unavailable for intermolecular interaction. In agreement, while the pThr peptide binding of an FHA domain typically consists of residues in the $\beta3-\beta4$, $\beta4-\beta5$, and $\beta6-\beta7$ loops (with the latter interacting mainly with the pT+3 residue),[6] no residue in the $\beta6-\beta7$ loop of TIFA FHA is involved in binding the pThr peptide.

Functional Support for the FHA−Ligand Interaction Revealed by the Structures. Previously, several site-specific mutants, including single mutants R51A and K88A, double mutant G50E/S66A, and triple mutant R51A/K88A/N89A, were shown to attenuate NF-κB activation.[20,22,24] The structural information described above can explain the effects of these mutants. Gly50 is well-known to be important for maintaining FHA domain structure.[6] Both Arg51 and Ser66 are involved in contacting the pThr peptide as shown in panels C and D of Figure 3. Lys88 and Asn89 are not directly involved in ligand binding; however, because they are located at the beginning of the $\beta6-\beta7$ loop, mutation of these residues may perturb the conformation.

On the basis of the structural information, we further tested the interaction between Ser53 and Glu5 by co-immunoprecipitation (co-IP) experiments *in vivo* as previously described.[24] We co-expressed Flag-tagged TIFA WT and Myc-tagged TIFA (WT or mutants) in HEK 293T cells and performed complementary co-IP experiments with Flag (Figure 3E, a) and with Myc (Figure 3E, b). The effects of WT-E5A and WT-S53A were clearly observed, supporting the functional importance of the Ser53−Glu5 interaction shown in Figure 3D. To further confirm that the changes in the WT-E5A and WT-S53A associations are related to FHA−pThr binding, we used ITC to show that binding of the E5A analogue of pThr9-$TIFA_{1-15}$ to WT TIFA is weakened by a factor of 5, and binding of pThr9-$TIFA_{1-15}$ to TIFA S53A is weakened by a factor of 10 (Figure 3F).

The Dimer Interface of TIFA Is Extensive and Separated from the pThr Binding Site. The full-length TIFA has been shown to exist as a dimer in solution based on size exclusion chromatography (SEC) and AUC analyses over a range of concentrations.[24] This property is fully supported by the crystal structures reported above. Because this dimeric property will be used to build a model for oligomerization described later, we further characterized the dimerization property in solution. As shown in panel a of Figure 4A, SEC−multiangle light scattering (MALS) analysis also shows that TIFA is monodispersed in solution with a calculated molecular weight of 44.15 kDa, which agrees with the theoretical molecular weight for dimers. In addition, AUC analyses indicate that TIFA (Figure 4A, b), truncated TIFA $tTIFA_{1-150}$ (c), and its complex with pThr9-$TIFA_{1-15}$ (d) all exist as dimers in solution.

In crystals, there is only one molecule in the asymmetry unit, which indicates that the $tTIFA_{1-150}$ dimer is symmetric. The two structures with different space groups (the apo form in $P3_221$ and the complex in $P4_232$) have the same dimer orientation and interface, suggesting that dimerization is not an artifact caused by crystallization. Two TIFA molecules contact each other via $\beta5$, $\beta6$, and $\beta9$, while the dyad axis is roughly perpendicular to the direction of $\beta5$ and $\beta6$, resulting in a head-to-tail arrangement between the two protomers (Figure 1H for the apo form and Figure 4B for the complex). As a result, the pThr peptide binding sites are at the opposite end, and the C-termini are distal from the dimerization interface. The dimer interface buries a solvent-accessible area of 917 Å^2, which is greater than that of a newly published Mdb1 FHA dimer[10] and involves hydrophobic interactions, van der Waals interactions, hydrogen bonding, and ionic bonds. These interactions at the dimer interface are reciprocal. There are 14 hydrogen or ionic bonds between seven pairs of residues: Lys76−Leu106 form a backbone hydrogen bond (Figure 4C, a); Tyr105−Glu135, Gln73−Lys88, Glu86−Lys108, and Gln73−Glu86 all form side chain hydrogen bonds or ionic bonds (Figure 4C, b); and Lys76−Asn107 and Leu74−Lys88 form hydrogen bonds between side chains and backbones (Figure 4C, a). Additional van der Waals contacts come from Lys76−Leu106, Phe75−Lys108, and Phe78−Leu103. These dimerization interface residues are contributed by $\beta5$, $\beta6$, the $\beta5-\beta6$ loop, and the $\beta8-\beta9$ loop. These results, along with that described in our previous report, suggest that TIFA is an intrinsic dimer with an extensive interface. In addition, it is important to note that the residues involved in the dimer interface are different from the residues involved in pThr binding shown in Figure 3C.

Mutations of Gln73, Glu86, and Lys108 to Ala (QEK mutant) should disrupt at least six hydrophilic interactions at the interface but were insufficient to break the dimer as shown by AUC (Figure 4D, a). In addition, its binding affinity for the pThr9-$TIFA_{1-15}$ peptide is similar to that of WT, based on the K_d measurement by Octet (Figure 4D, b). These additional data support that even disruption of six hydrophilic interactions is unable to break the dimer, and that it is possible to disrupt interfacial interactions (though the dimer is still intact) without affecting the pThr binding ability. On the other hand, the dimer folding could be destabilized by more extensive mutations, as Q73A/E86A/K88A/K108A, Q73A/E86A/K88A/K108A/E135A, and Q73K/E86K/E135A mutants could not be purified in stable forms.

The Dimer of TIFA FHA Is Unique among FHA Domains. One of the main functions of FHA domains is to mediate dimerization between two monomers via pThr−FHA domain binding in many cases, leading to, for example, autophosphorylation and activation of CHK2-like kinases.[17] Thus, FHA domains usually exist in monomers, except that the MDC1 FHA domain[14,15] and the CHK2 FHA domain[41] are in equilibrium between monomer and dimer in solution. Dimeric crystal structures have been reported for the FHA domain of MDC1[14−16] and the FHA-kinase domains of CHK2,[17] but their dimer interface areas, 472 Å^2 for the MDC1 FHA domain and 760 Å^2 for the CHK2 FHA domain, are smaller than that of the TIFA FHA domain (917 Å^2 as mentioned above). Furthermore, unlike TIFA, the dimer interfaces of the MDC1 FHA domain and CHK2 FHA domain are contributed mainly through van der Waals interactions between hydrophobic residues. The diverse properties in the FHA domain dimerization reflect the lack of conserved sequences within the β-strands in the FHA domain family. Although the β-sandwich structure of FHA domain is conserved in the family, the dimers of the FHA domains of TIFA, MDC1, and CHK2 are built in different ways: TIFA dimerizes via $\beta5$, $\beta6$, and $\beta9$; MDC1 FHA via $\beta10$, $\beta11$, and $\beta7$ (head-to-tail); and CHK2 FHA via $\beta1$, $\beta2$, and $\beta11$ (head-to-head). Taken together, the results suggest that the TIFA FHA domain differs from the MDC1 FHA domain and CHK2 FHA domain in that it forms intrinsic dimers, in the absence of any phosphorylation. This unique property is highly relevant to the function of TIFA.

Structural Basis for the Important Function of TIFA Oligomerization. We recently demonstrated that TIFA oligomerization is dependent on the FHA−pT9 interaction,

DOI: 10.1021/acs.biochem.5b00500
Biochemistry 2015, 54, 6219−6229

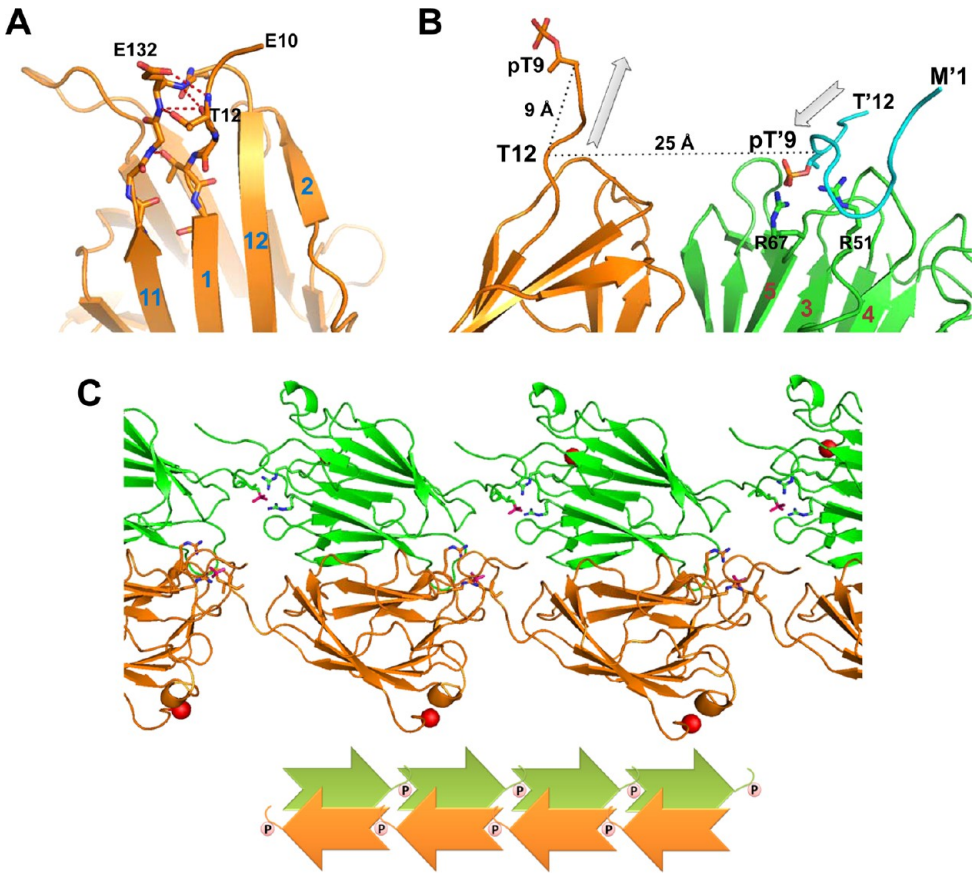

Figure 5. Structural basis for the important function of TIFA oligomerization. (A) Interactions between Thr12 and the β11−β12 loop. (B) Structural illustration for the unfeasibility of intradimer pThr−FHA domain binding. The side chain of pThr9 is shown as sticks. (C) Model for the dimer−dimer interaction via pThr9−FHA domain binding. The red sphere indicates the C-terminus, and the red x indicates pThr9. Arg51 and Arg67 are shown as sticks.

by showing that TNFα-treated cell lysate enhances TIFA Thr9 phosphorylation, TIFA oligomerization, and NF-κB activation, and that these effects were muted by mutation of the pThr site (T9A) or the putative pThr binding residues.[24] By showing that TIFA is an intrinsic dimer in the absence of phosphorylation, our results support the idea that TIFA oligomerization occurs via the FHA−pT binding between dimers of TIFA. In fact, after examination of the structural detail of $tTIFA_{1-150}$-pThr9-$TIFA_{1-15}$, it is clear that the pThr peptide of the complex must come from another TIFA dimer rather than from the neighboring protomer within the dimer, for the following reasons. (a) As shown by the sequence alignment in Figure 2, the N-terminal segment is relatively short in TIFA compared to other FHA domain-containing proteins that have a pThr site preceding the FHA domain.[3,13−15,17,39] These N-terminal segments are usually unstructured and not traceable in crystal structures. However, in the $tTIFA_{1-150}$ crystal structure, the electron density after Glu10 could be clearly discerned, and the residues from Thr12 to the start of the strand β1 at Cys15 are in contact with the β11−β12 loop (Figure 5A). These factors make it impossible for Thr9 of the left protomer (9 Å from Thr12) to reach the binding pocket of the right protomer (25 Å away) (Figure 5B). (b) As shown by the arrows in Figure 5B, the segment from Thr12 to Thr9 in the left protomer is pointing outward, whereas that of the pThr peptide bound to the right protomer is pointing inward. Thus, the bound pThr9-$TIFA_{1-15}$ peptide cannot come from the N-terminus of the other protomer on the basis of not only distance but also orientation.

On the basis of these results and analyses, we propose a structural model for the interdimer binding and propagation, in which one dimer interacts with the next dimer via an "anti-parallel pair" of "head-to-tail binding" between pThr9 and the FHA domain, allowing the C-terminal region (red ball) to be exposed on the same side for TRAF6 binding (Figure 5C). The proposed model provides a scaffold to facilitate the signal cascade mediated by association of TRAF6, which has been suggested to occur constitutively involving Glu178 of TIFA.[20] Similar to Hao Wu's TRAF6 model that has the potential for infinite propagation,[42] TIFA oligomerization could also propagate continuously through pThr−FHA domain interaction.

■ CONCLUSION

Overall, our results reveal a novel FHA domain that has a unique architecture, a noncanonical pThr peptide binding mode, a distinct dimer interface, and a novel mechanism for mediating oligomerization. These features broaden the structural and functional diversities of the FHA domain. The structural information about TIFA and the mechanism of FHA domain-mediated interdimer oligomerization should be useful for our understanding of the mechanism of TRAF6 oligomerization in immune responses, and the signaling pathways leading to NF-κB activation.

DOI: 10.1021/acs.biochem.5b00500
Biochemistry 2015, 54, 6219−6229

■ ASSOCIATED CONTENT

Accession Codes

Coordinates and structure factors have been deposited as Protein Data Bank entries 4ZGI for $tTIFA_{1-150}$ and 4YM4 for $tTIFA_{1-150}$-pThr9-$TIFA_{1-15}$.

■ AUTHOR INFORMATION

Corresponding Author

*E-mail: mdtsai@gate.sinica.edu.tw. Phone: 886-2-27855696-3070.

Funding

The work was funded by the National Health Research Institute and Academia Sinica.

Notes

The authors declare no competing financial interest.

■ ACKNOWLEDGMENTS

This work was supported by the National Health Research Institute and Academia Sinica. We thank the National Synchrotron Radiation Research Center (NSRRC) for access to beamlines BL13C, BL13B, and BL15A and SPring-8 for access to beamlines BL12B2 and BL44XU. We also thank Academia Sinica and Ministry of Science and Technology for the support of crystallization, mass spectrometry, and biophysical facilities.

■ ABBREVIATIONS

AUC, analytical ultracentrifugation; FHA domain, Forkhead-associated (FHA) domain; NF-κB, nuclear factor κB; MAD, multiple-wavelength anomalous dispersion; MR, molecular replacement; PDB, Protein Data Bank; pThr, phosphothreonine; SAD, single-wavelength anomalous dispersion; SEC−MALS, size exclusion chromatography−multiangle light scattering; TIFA, TRAF-interacting protein with a FHA domain; TNF-α, tumor necrosis factor-α; TRAF6, tumor necrosis factor (TNF) receptor-associated factor (TRAF)-6.

■ REFERENCES

(1) Hofmann, K., and Bucher, P. (1995) The FHA domain: a putative nuclear signalling domain found in protein kinases and transcription factors. *Trends in biochemical sciences 20*, 347−349.

(2) Liao, H., Byeon, I. J., and Tsai, M. D. (1999) Structure and function of a new phosphopeptide-binding domain containing the FHA2 of Rad53. *J. Mol. Biol. 294*, 1041−1049.

(3) Durocher, D., Taylor, I. A., Sarbassova, D., Haire, L. F., Westcott, S. L., Jackson, S. P., Smerdon, S. J., and Yaffe, M. B. (2000) The molecular basis of FHA domain:phosphopeptide binding specificity and implications for phospho-dependent signaling mechanisms. *Mol. Cell 6*, 1169−1182.

(4) Durocher, D., Henckel, J., Fersht, A. R., and Jackson, S. P. (1999) The FHA domain is a modular phosphopeptide recognition motif. *Mol. Cell 4*, 387−394.

(5) Liao, H., Yuan, C., Su, M. I., Yongkiettrakul, S., Qin, D., Li, H., Byeon, I. J., Pei, D., and Tsai, M. D. (2000) Structure of the FHA1 domain of yeast Rad53 and identification of binding sites for both FHA1 and its target protein Rad9. *J. Mol. Biol. 304*, 941−951.

(6) Mahajan, A., Yuan, C. H., Lee, H., Chen, E. S. W., Wu, P. Y., and Tsai, M. D. (2008) Structure and Function of the Phosphothreonine-Specific FHA Domain. *Sci. Signaling 1*, re12.

(7) Durocher, D., and Jackson, S. P. (2002) The FHA domain. *FEBS Lett. 513*, 58−66.

(8) Coquelle, N., and Glover, J. N. (2010) FHA domain pThr binding specificity: it's all about me. *Structure 18*, 1549−1550.

(9) Raasch, K., Bocola, M., Labahn, J., Leitner, A., Eggeling, L., and Bott, M. (2014) Interaction of 2-oxoglutarate dehydrogenase OdhA with its inhibitor OdhI in Corynebacterium glutamicum: Mutants and a model. *J. Biotechnol. 191*, 99−105.

(10) Luo, S., Xin, X., Du, L. L., Ye, K., and Wei, Y. (2015) Dimerization mediated by a divergent FHA domain is essential for the DNA damage and spindle functions of fission yeast Mdb1. *J. Biol. Chem.*,.

(11) Pennell, S., Westcott, S., Ortiz-Lombardia, M., Patel, D., Li, J., Nott, T. J., Mohammed, D., Buxton, R. S., Yaffe, M. B., Verma, C., and Smerdon, S. J. (2010) Structural and functional analysis of phosphothreonine-dependent FHA domain interactions. *Structure 18*, 1587−1595.

(12) Hammet, A., Pike, B. L., McNees, C. J., Conlan, L. A., Tenis, N., and Heierhorst, J. (2003) FHA domains as phospho-threonine binding modules in cell signaling. *IUBMB Life 55*, 23−27.

(13) Barthe, P., Roumestand, C., Canova, M. J., Kremer, L., Hurard, C., Molle, V., and Cohen-Gonsaud, M. (2009) Dynamic and structural characterization of a bacterial FHA protein reveals a new auto-inhibition mechanism. *Structure 17*, 568−578.

(14) Liu, J., Luo, S., Zhao, H., Liao, J., Li, J., Yang, C., Xu, B., Stern, D. F., Xu, X., and Ye, K. (2012) Structural mechanism of the phosphorylation-dependent dimerization of the MDC1 forkhead-associated domain. *Nucleic Acids Res. 40*, 3898−3912.

(15) Jungmichel, S., Clapperton, J. A., Lloyd, J., Hari, F. J., Spycher, C., Pavic, L., Li, J., Haire, L. F., Bonalli, M., Larsen, D. H., Lukas, C., Lukas, J., MacMillan, D., Nielsen, M. L., Stucki, M., and Smerdon, S. J. (2012) The molecular basis of ATM-dependent dimerization of the Mdc1 DNA damage checkpoint mediator. *Nucleic Acids Res. 40*, 3913−3928.

(16) Wu, H. H., Wu, P. Y., Huang, K. F., Kao, Y. Y., and Tsai, M. D. (2012) Structural delineation of MDC1-FHA domain binding with CHK2-pThr68. *Biochemistry 51*, 575−577.

(17) Cai, Z., Chehab, N. H., and Pavletich, N. P. (2009) Structure and activation mechanism of the CHK2 DNA damage checkpoint kinase. *Mol. Cell 35*, 818−829.

(18) Xu, Q., Deller, M. C., Nielsen, T. K., Grant, J. C., Lesley, S. A., Elsliger, M. A., Deacon, A. M., and Wilson, I. A. (2014) Structural insights into the recognition of phosphopeptide by the FHA domain of kanadaptin. *PLoS One 9*, e107309.

(19) Kanamori, M., Suzuki, H., Saito, R., Muramatsu, M., and Hayashizaki, Y. (2002) T2BP, a novel TRAF2 binding protein, can activate NF-kappaB and AP-1 without TNF stimulation. *Biochem. Biophys. Res. Commun. 290*, 1108−1113.

(20) Takatsuna, H., Kato, H., Gohda, J., Akiyama, T., Moriya, A., Okamoto, Y., Yamagata, Y., Otsuka, M., Umezawa, K., Semba, K., and Inoue, J. (2003) Identification of TIFA as an adapter protein that links tumor necrosis factor receptor-associated factor 6 (TRAF6) to interleukin-1 (IL-1) receptor-associated kinase-1 (IRAK-1) in IL-1 receptor signaling. *J. Biol. Chem. 278*, 12144−12150.

(21) Ding, N., Zhang, Y., Loughran, P. A., Wang, Q., Tsung, A., and Billiar, T. R. (2013) TIFA upregulation after hypoxia-reoxygenation is TLR4- and MyD88-dependent and associated with HMGB1 upregulation and release. *Free Radical Biol. Med. 63*, 361−367.

(22) Ea, C. K., Sun, L., Inoue, J., and Chen, Z. J. (2004) TIFA activates IkappaB kinase (IKK) by promoting oligomerization and ubiquitination of TRAF6. *Proc. Natl. Acad. Sci. U. S. A. 101*, 15318−15323.

(23) Gaudet, R. G., Sintsova, A., Buckwalter, C. M., Leung, N., Cochrane, A., Li, J., Cox, A. D., Moffat, J., and Gray-Owen, S. D. (2015) Cytosolic detection of the bacterial metabolite HBP activates TIFA-dependent innate immunity. *Science 348*, 1251−1255.

(24) Huang, C. C., Weng, J. H., Wei, T. Y., Wu, P. Y., Hsu, P. H., Chen, Y. H., Wang, S. C., Qin, D., Hung, C. C., Chen, S. T., Wang, A. H., Shyy, J. Y., and Tsai, M. D. (2012) Intermolecular binding between TIFA-FHA and TIFA-pT mediates tumor necrosis factor alpha stimulation and NF-kappaB activation. *Molecular and cellular biology 32*, 2664−2673.

DOI: 10.1021/acs.biochem.5b00500
Biochemistry 2015, 54, 6219−6229

(25) Otwinowski, O., and Minor, W. (1997) Processing of X-ray Diffraction Data Collected in Oscillation Mode. *Methods Enzymol. 276*, 307−326.
(26) Sheldrick, G. M. (2010) Experimental phasing with SHELXC/D/E: combining chain tracing with density modification. *Acta Crystallogr., Sect. D: Biol. Crystallogr. 66*, 479−485.
(27) McCoy, A. J., Grosse-Kunstleve, R. W., Adams, P. D., Winn, M. D., Storoni, L. C., and Read, R. J. (2007) Phaser crystallographic software. *J. Appl. Crystallogr. 40*, 658−674.
(28) Cowtan, K. D., and Zhang, K. Y. (1999) Density modification for macromolecular phase improvement. *Prog. Biophys. Mol. Biol. 72*, 245−270.
(29) Chen, C. D., Huang, Y. C., Chiang, H. L., Hsieh, Y. C., Guan, H. H., Chuankhayan, P., and Chen, C. J. (2014) Direct phase selection of initial phases from single-wavelength anomalous dispersion (SAD) for the improvement of electron density and ab initio structure determination. *Acta Crystallogr., Sect. D: Biol. Crystallogr. 70*, 2331−2343.
(30) Cowtan, K. (2006) The Buccaneer software for automated model building. 1. Tracing protein chains. *Acta Crystallogr., Sect. D: Biol. Crystallogr. 62*, 1002−1011.
(31) Collaborative Computational Project, Number 4 (1994) The CCP4 suite: programs for protein crystallography. *Acta Crystallogr., Sect. D: Biol. Crystallogr. 50*, 760−763.
(32) Emsley, P., and Cowtan, K. (2004) Coot: model-building tools for molecular graphics. *Acta Crystallogr., Sect. D: Biol. Crystallogr. 60*, 2126−2132.
(33) Murshudov, G. N., Skubak, P., Lebedev, A. A., Pannu, N. S., Steiner, R. A., Nicholls, R. A., Winn, M. D., Long, F., and Vagin, A. A. (2011) REFMAC5 for the refinement of macromolecular crystal structures. *Acta Crystallogr., Sect. D: Biol. Crystallogr. 67*, 355−367.
(34) Adams, P. D., Afonine, P. V., Bunkoczi, G., Chen, V. B., Davis, I. W., Echols, N., Headd, J. J., Hung, L. W., Kapral, G. J., Grosse-Kunstleve, R. W., McCoy, A. J., Moriarty, N. W., Oeffner, R., Read, R. J., Richardson, D. C., Richardson, J. S., Terwilliger, T. C., and Zwart, P. H. (2010) PHENIX: a comprehensive Python-based system for macromolecular structure solution. *Acta Crystallogr., Sect. D: Biol. Crystallogr. 66*, 213−221.
(35) *The PyMOL Molecular Graphics System*, version 1.7.4, Schrödinger, LLC, Portland, OR.
(36) Soding, J., Biegert, A., and Lupas, A. N. (2005) The HHpred interactive server for protein homology detection and structure prediction. *Nucleic Acids Res. 33*, W244−248.
(37) Inoue, J., Yagi, S., Ishikawa, K., Azuma, S., Ikawa, S., and Semba, K. (2005) Identification and characterization of Xenopus laevis homologs of mammalian TRAF6 and its binding protein TIFA. *Gene 358*, 53−59.
(38) Minoda, Y., Saeki, K., Aki, D., Takaki, H., Sanada, T., Koga, K., Kobayashi, T., Takaesu, G., and Yoshimura, A. (2006) A novel Zinc finger protein, ZCCHC11, interacts with TIFA and modulates TLR signaling. *Biochem. Biophys. Res. Commun. 344*, 1023−1030.
(39) Lee, H., Yuan, C., Hammet, A., Mahajan, A., Chen, E. S., Wu, M. R., Su, M. I., Heierhorst, J., and Tsai, M. D. (2008) Diphospho-threonine-specific interaction between an SQ/TQ cluster and an FHA domain in the Rad53-Dun1 kinase cascade. *Mol. Cell 30*, 767−778.
(40) Li, H., Byeon, I.-J. L., Ju, Y., and Tsai, M.-D. (2004) Structure of Human Ki67 FHA Domain and its Binding to a Phosphoprotein Fragment from hNIFK Reveal Unique Recognition Sites and New Views to the Structural Basis of FHA Domain Functions. *J. Mol. Biol. 335*, 371−381.
(41) Li, J., Taylor, I. A., Lloyd, J., Clapperton, J. A., Howell, S., MacMillan, D., and Smerdon, S. J. (2008) Chk2 oligomerization studied by phosphopeptide ligation: implications for regulation and phosphodependent interactions. *J. Biol. Chem. 283*, 36019−36030.
(42) Yin, Q., Lin, S. C., Lamothe, B., Lu, M., Lo, Y. C., Hura, G., Zheng, L., Rich, R. L., Campos, A. D., Myszka, D. G., Lenardo, M. J., Darnay, B. G., and Wu, H. (2009) E2 interaction and dimerization in the crystal structure of TRAF6. *Nat. Struct. Mol. Biol. 16*, 658−666.
(43) Williams, R. S., Dodson, G. E., Limbo, O., Yamada, Y., Williams, J. S., Guenther, G., Classen, S., Glover, J. N., Iwasaki, H., Russell, P., and Tainer, J. A. (2009) Nbs1 flexibly tethers Ctp1 and Mre11-Rad50 to coordinate DNA double-strand break processing and repair. *Cell 139*, 87−99.
(44) Alderwick, L. J., Molle, V., Kremer, L., Cozzone, A. J., Dafforn, T. R., Besra, G. S., and Futterer, K. (2006) Molecular structure of EmbR, a response element of Ser/Thr kinase signaling in Mycobacterium tuberculosis. *Proc. Natl. Acad. Sci. U. S. A. 103*, 2558−2563.
(45) Ali, A. A., Jukes, R. M., Pearl, L. H., and Oliver, A. W. (2009) Specific recognition of a multiply phosphorylated motif in the DNA repair scaffold XRCC1 by the FHA domain of human PNK. *Nucleic Acids Res. 37*, 1701−1712.
(46) Huen, M. S., Grant, R., Manke, I., Minn, K., Yu, X., Yaffe, M. B., and Chen, J. (2007) RNF8 transduces the DNA-damage signal via histone ubiquitylation and checkpoint protein assembly. *Cell 131*, 901−914.

DOI: 10.1021/acs.biochem.5b00500
Biochemistry 2015, 54, 6219−6229